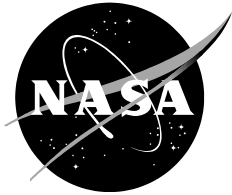


NASA/TM—2019–220304



TESS Data Release Notes: Sector 11, DR16

*Michael M. Fausnaugh, Christopher J. Burke
Kavli Institute for Astrophysics and Space Science, Massachusetts Institute of Technology,
Cambridge, Massachusetts*

*Douglas A. Caldwell
SETI Institute, Mountain View, California*

*Jon M. Jenkins
Ames Research Center, Moffett Field, California*

*Jeffrey C. Smith, Joseph D. Twicken
SETI Institute, Mountain View, California*

*Roland Vanderspek
Kavli Institute for Astrophysics and Space Science, Massachusetts Institute of Technology,
Cambridge, Massachusetts*

*John P. Doty
Noqsi Aerospace Ltd, Billerica, Massachusetts*

*Eric B. Ting
Ames Research Center, Moffett Field, California*

*Joel S. Villaseñor
Kavli Institute for Astrophysics and Space Science, Massachusetts Institute of Technology,
Cambridge, Massachusetts*

June 19, 2019

Acknowledgements

These Data Release Notes provide information on the processing and export of data from the Transiting Exoplanet Survey Satellite (TESS). The data products included in this data release are full frame images (FFIs), target pixel files, light curve files, collateral pixel files, cotrending basis vectors (CBVs), and Data Validation (DV) reports, time series, and associated xml files.

These data products were generated by the TESS Science Processing Operations Center (SPOC, [Jenkins et al., 2016](#)) at NASA Ames Research Center from data collected by the TESS instrument, which is managed by the TESS Payload Operations Center (POC) at Massachusetts Institute of Technology (MIT). The format and content of these data products are documented in the [Science Data Products Description Document \(SDPDD\)](#)¹. The SPOC science algorithms are based heavily on those of the Kepler Mission science pipeline, and are described in the Kepler Data Processing Handbook ([Jenkins, 2017](#)).² The Data Validation algorithms are documented in [Twicken et al. \(2018\)](#) and [Li et al. \(2019\)](#). The TESS Instrument Handbook ([Vanderspek et al., 2018](#)) contains more information about the TESS instrument design, detector layout, data properties, and mission operations.

The TESS Mission is funded by NASA's Science Mission Directorate.

This report is available in electronic form at
<https://archive.stsci.edu/tess/>

¹<https://archive.stsci.edu/missions/tess/doc/EXP-TESS-ARC-ICD-TM-0014.pdf>

²<https://archive.stsci.edu/kepler/manuals/KSCI-19081-002-KDPH.pdf>

1 Observations

TESS Sector 11 observations include physical orbits 29 and 30 of the spacecraft around the Earth. The use of Camera 1 in attitude control was disabled at the start of both orbits due to strong scattered light signals. Data collection was paused for 1.08 days during perigee passage while downloading data. In total, there are 26.04 days of science data collected in Sector 11.

Table 1: Sector 11 Observation times

	UTC	TJD ^a	Cadence #
Orbit 29 start	2019-04-23 06:29:32	1596.77203	265908
Camera 1 guiding enabled	2019-04-26 10:33:32	1599.94148	268190
Orbit 29 end	2019-05-06 04:37:32	1609.69425	275212
Orbit 30 start	2019-05-07 06:35:32	1610.77620	275991
Camera 1 guiding enabled	2019-05-10 16:43:32	1614.19842	278455
Orbit 30 end	2019-05-20 09:21:31	1623.89147	285434

^a TJD = TESS JD = JD - 2,457,000.0

The spacecraft was pointing at RA (J2000): 189.124736°; Dec (J2000): -65.536906°; Roll: 138.076125°. Two-minute cadence data were collected for 20,000 targets, and full frame images were collected every 30 minutes. See the TESS project [Sector 11 observation page](#)³ for the coordinates of the spacecraft pointing and center field-of-view of each camera, as well as the detailed target list. Fields-of-view for each camera and the Guest Investigator two-minute target list can be found at the TESS Guest Investigator Office [observations status page](#)⁴.

1.1 Notes on Individual Targets

Ten very bright stars ($T_{\text{mag}} \lesssim 1.8$) with large pixel stamps were not processed in the photometric pipeline. Target pixel files with raw data are provided, but no light curves were produced. The affected TIC IDs are 272314138, 399646462, 471011144, 471011145, 38877693, 179323446, 440960978, 30247429, 328329822, and 396139114.

Two target stars (300015238 and 300015239) are blended with each other—the contaminating flux for these objects is very large, and the resulting photometry for such targets is expected to be unreliable.

Eight bright ($T_{\text{mag}} \lesssim 3.4$), saturated, bleeding targets (148415949, 290794924, 333947284, 333950446, 390442076, 450568754, 453885273, 460532958) had selected pixel stamps that did not fully capture the bleed trails.

³<https://tess.mit.edu/observations/sector-11>

⁴<https://heasarc.gsfc.nasa.gov/docs/tess/status.html>

1.2 Spacecraft Pointing and Momentum dumps

The reaction wheel speeds were reset with momentum dumps every 3.125 days. Figure 1 summarizes the pointing performance over the course of the sector based on Fine Pointing telemetry.

At the start of each orbit, the Earth was close to the boresight of Camera 1, and the level of scattered light was too high for meaningful guide star centroids to be measured. Guiding with Camera 1 was therefore disabled at these times, and attitude control was done using only inputs from Camera 4. When Camera 1 guiding was re-enabled, the spacecraft attitude shifted by a small amount, about 1 arc-second (0.05 pixels).

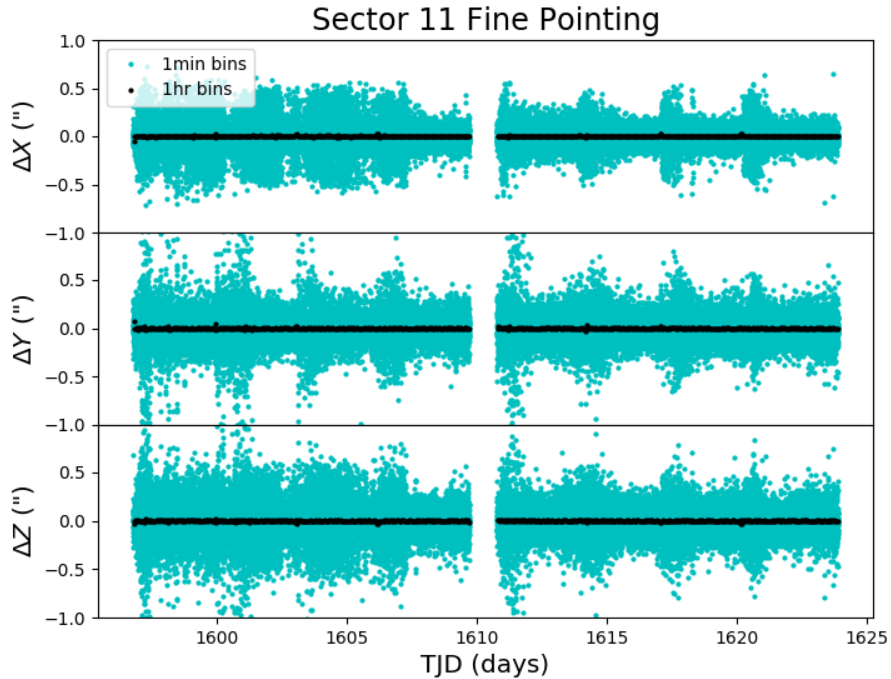


Figure 1: Guiding corrections based on spacecraft fine pointing telemetry. The delta-quaternions from each camera have been converted to spacecraft frame, binned to 1 minute and 1 hour, and averaged across cameras. Long-term trends (such as those caused by differential velocity aberration) have also been removed. The $\Delta X/\Delta Y$ directions represent offsets along the detectors' rows/columns, while the ΔZ direction represents spacecraft roll.

1.3 Scattered Light

Figure 2 shows the median value of the background estimate for all targets on a given CCD as a function of time. Figure 3 shows the angle between each camera's boresight and the Earth or Moon—this figure can be used to identify periods affected by scattered light and the relative contributions of the Earth and Moon to the image backgrounds. In Sector 11, the main stray light features are caused by the Earth at the start of each orbit.

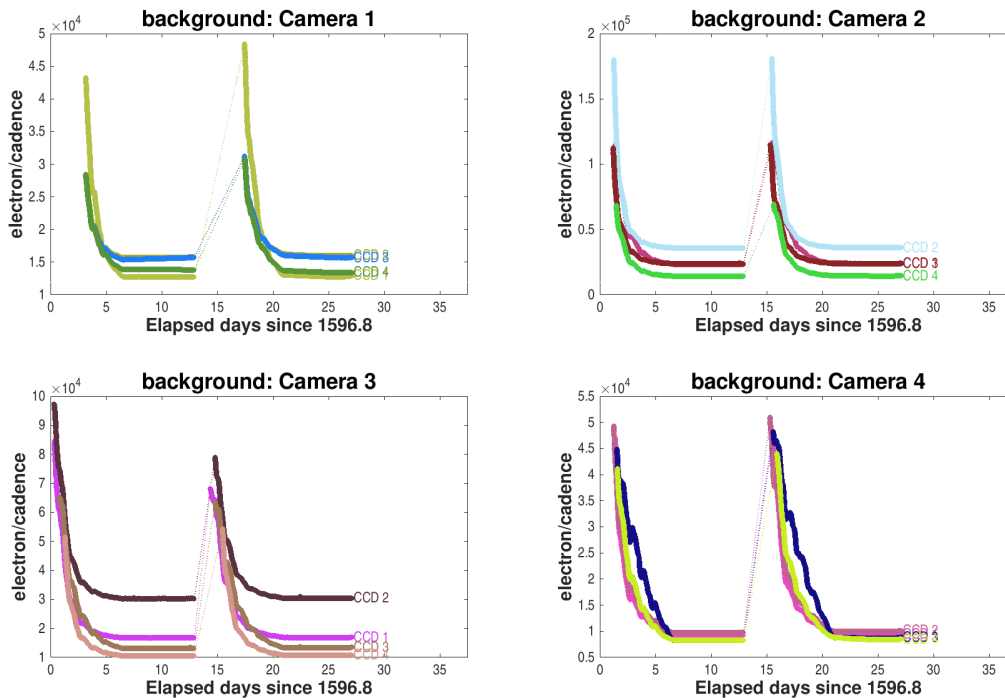


Figure 2: Median background flux across all targets on a given CCD in each camera. The changes are caused by variations in the orientation and distance of the Earth and Moon.

2 Data Anomaly Flags

See the SDPDD (§9) for a list of data quality flags and the associated binary values used for TESS data, and the TESS Instrument Handbook for a more detailed description of each flag.

The following flags were not used in Sector 11: bits 2, 7, 9, and 11 (Safe Mode, Cosmic Ray in Aperture, Discontinuity, Cosmic Ray in Collateral Pixel).

Cadences marked with bits 1, 3, 4, 6, and 12 (Attitude Tweak, Coarse Point, Earth Point, Reaction Wheel Desaturation Event, and Straylight) were marked based on spacecraft telemetry.

Cadences marked with bit 5 and 10 (Argabrightening Events and Impulsive Outlier) were identified by the SPOC pipeline. Bit 5 marks a sudden change in the background measurements. In practice, bit 5 flags are caused by rapidly changing glints and unstable pointing at times near momentum dumps. Bit 10 marks an outlier identified by PDC and omitted from the cotrending procedure.

Cadences marked with bit 8 (Manual Exclude) are ignored by PDC, TPS, and DV for cotrending and transit searches. In Sector 11, these cadences were identified using spacecraft telemetry from the fine pointing system. All cadences with pointing excursions >21 arcseconds (~ 1 pixel) were flagged for manual exclude. See Figure 4 for an assessment of the performance of the cotrending based on the final set of manual excludes.

In addition, strong scattered light signals affected the systematic error removal in PDC

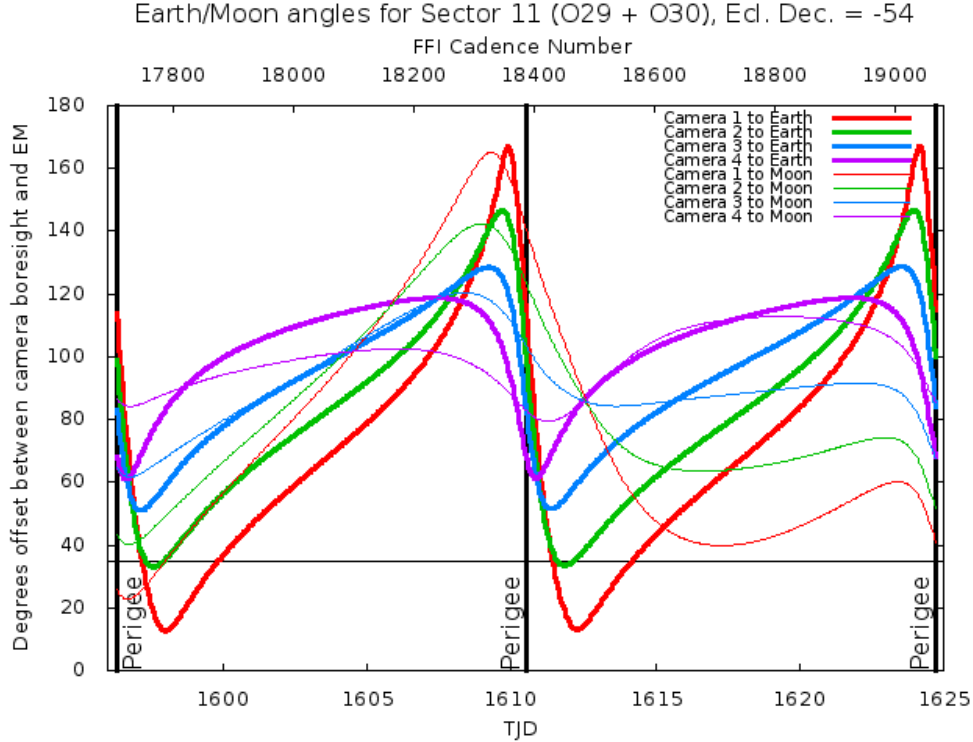


Figure 3: Angle between the four camera boresights and the Earth/Moon as a function of time. When the Earth/Moon moves within 37° of a camera’s boresight, scattered light patterns and complicated features such as glints may appear. At larger angles, low level patchy features may appear. This figure can be used to identify periods affected by scattered light and the relative contributions of the Earth and Moon to the background. However, the background intensity and locations of scattered light features depend on additional factors, such as the Earth/Moon azimuth and distance from the spacecraft.

and the planet search in TPS. Cadences during this time were excluded from the pipeline analysis. The time periods for these exclusions are variable per CCD, and the corresponding cadence ranges are given in Table 2. Raw and flux-calibrated (without background correction) pixels for these cadences are provided in the target pixel files, but no photometry or centroid positions were calculated. The pipeline exports do not support data quality flags on a per CCD basis, and so the QUALITY column is not marked beyond the flags described above.

FFIs were only marked with bits 6 and 12 (Reaction Wheel Desaturation Events and Straylight). Only one FFI is affected by each momentum dump.

3 Anomalous Effects

3.1 Smear Correction Issues

The following columns were impacted by bright stars in the science frame and/or the upper buffer rows, which bleed into the upper serial register resulting in an overestimated smear

Table 2: Cadence ranges for data excludes due to scattered light

Cam	CCD	Orbit 29	Orbit 30
1	1	265908–268190	275991–278455
1	2	265908–268190	275991–278455
1	3	265908–268190	275991–278455
1	4	265908–268190	275991–278455
2	1	265908–266909	275991–277085
2	2	265908–266808	275991–277028
2	3	265908–266769	275991–276933
2	4	265908–266961	275991–277153
3	1	265908–266150	275991–276250
3	2	265908–266141	275991–276539
3	3	265908–266446	275991–276531
3	4	265908–266841	275991–277043
4	1	265908–266900	275991–277090
4	2	265908–266810	275991–276909
4	3	265908–267023	275991–277135
4	4	265908–267052	275991–277374

correction.

- Camera 1, CCD 3, Column 224, Star ϕ^1 Lupi
- Camera 2, CCD 2, Column 1700, Star System α Centauri

In addition, Camera 1, CCD 3, Column 1248 (slice C) is impacted by intra-camera crosstalk from the bright star ϕ^1 Lupi located on slice A (see Section 6.8.6 of the TESS Instrument Handbook).

3.2 Fireflies and Fireworks

Table 3 lists all firefly and fireworks events for Sector 11. These phenomena are small, spatially extended, comet-like features in the images—created by sunlit particles in the camera FOV—that may appear one or two at a time (fireflies) or in large groups (fireworks). See the TESS Instrument Handbook for a more complete description.

4 Pipeline Performance and Results

4.1 Light Curves and Photometric Precision

Figure 5 gives the PDC goodness metrics for residual correlation and introduced noise on a scale between 0 (bad) and 1 (good). The performance of PDC is very good and generally uniform over most of the field of view. There is some residual correlation in Camera 1, which appears to be an artifact caused by the gaps described in §2 and the Attitude Tweak flag

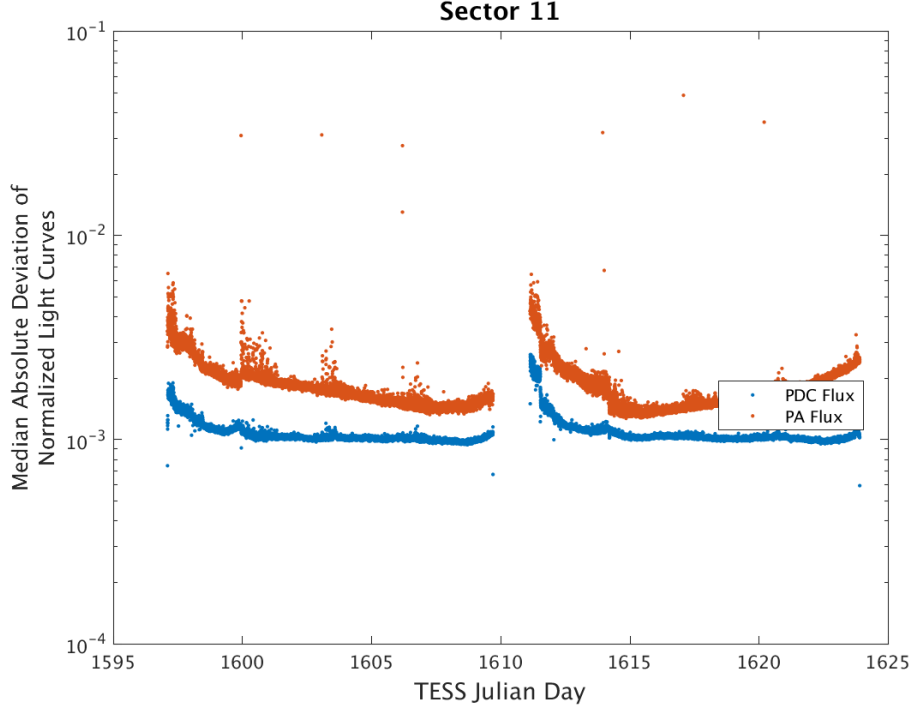


Figure 4: Median absolute deviation (MAD) for the 2-minute cadence data from Sector 11, showing the performance of the cotrending after identifying Manual Exclude data quality flags. The MAD is calculated in each cadence across stars with flux variations less than 1% for both the PA (red) and PDC (blue) light curves, where each light curve is normalized by its median flux value. The scatter in the PA light curves is much higher than that for the PDC light curves, and the outliers in the PA light curves are largely absent from the PDC light curves due to the use of the anomaly flags. Note that the first and last cadences in each orbit are treated as gaps by PDC.

in orbit 30. In some cases, the combination of these flags produces two different mean flux levels in the first and second orbits. However, the offset is always very small and affects a minority of targets. There are some other residual issues in the crowded fields that make up the plane of the Galaxy. Figure 6 shows the achieved Combined Differential Photometric Precision (CDPP) at 1-hour timescales for all targets.

4.2 Transit Search and Data Validation

In Sector 11, the light curves of 19990 targets were subjected to the transit search in TPS. Of these, Threshold Crossing Events (TCEs) at the 7.1σ level were generated for 1198 targets.

The top panel of Figure 7 shows the distribution of orbital periods for the TPS TCEs found in Sector 11. There is an excess of TCEs in the orbital period distribution at 14 days. Figure 8 shows the number of TCEs at a given cadence that exhibit a transit signal—the spacing between peaks accounts for the preferred periods in Figure 7. In Sector 11, the excess TCEs at 14 days are mainly caused by complicated backgrounds and glints at the beginning of each orbit.

The vertical histogram in the right panel of Figure 7 shows the distribution of tran-

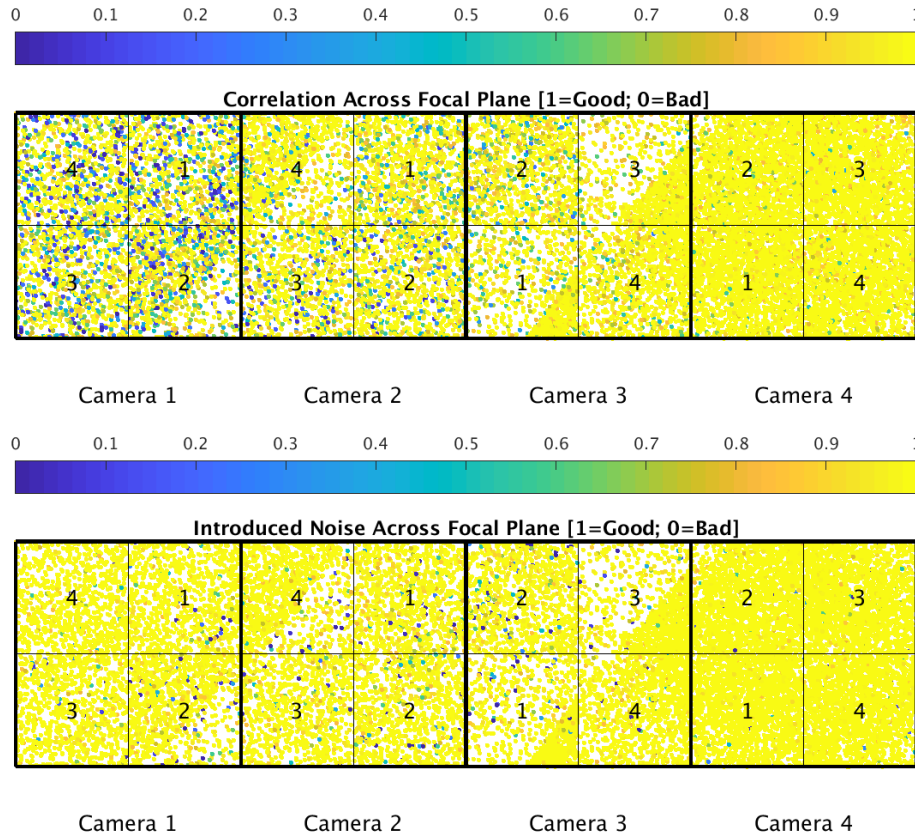


Figure 5: PDC residual correlation goodness metric (top panel) and PDC introduced noise goodness metric (bottom panel). The metric values are shown on a focal plane map indicating the camera and CCD location of each target. The correlation goodness metric is calibrated such that a value greater than 0.8 means there is less than 10% mean absolute correlation between the target under study and all other targets on the CCD. The introduced noise metric is calibrated such that a value greater than 0.8 means the power in broad-band introduced noise is below the level of uncertainties in the flux values.

sit depths derived from limb-darkened transiting planet model fits for TCEs. The model transit depths range down to the order of 100 ppm, but the bulk of the transit depths are considerably larger.

A search for additional TCEs in potential multiple planet systems was conducted in DV through calls to TPS. A total of 1648 TCEs were ultimately identified in the SPOC pipeline on 1198 unique target stars. Table 4 provides a breakdown of the number of TCEs by target. Note that targets with large numbers of TCEs are likely to include false positives.

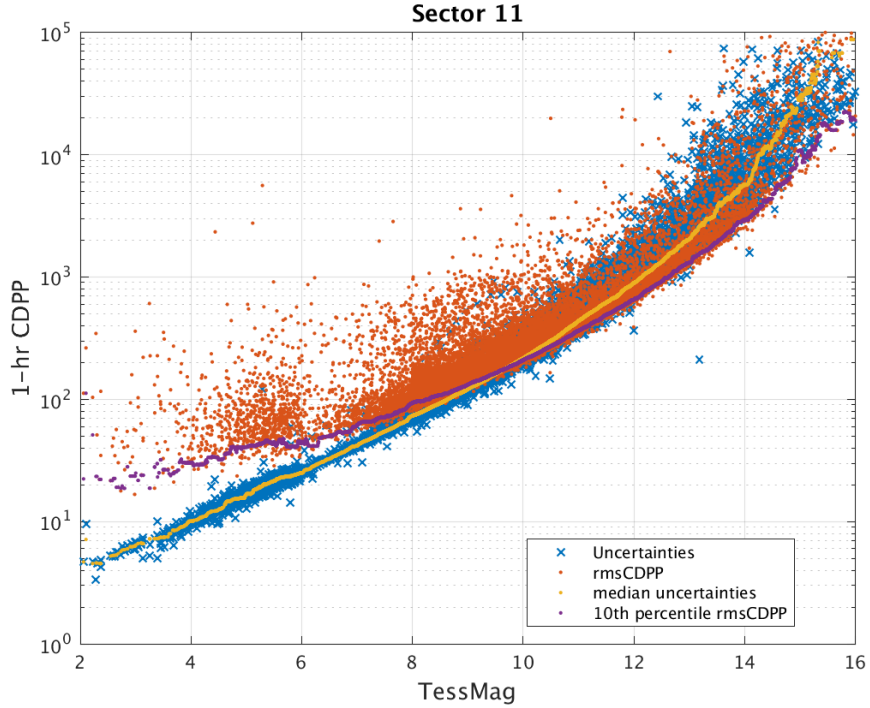


Figure 6: 1-hour CDPP. The red points are the RMS CDPP measurements for the 19990 light curves from Sector 11 plotted as a function of TESS magnitude. The blue x's are the uncertainties, scaled to 1-hour timescale. The purple curve is a moving 10th percentile of the RMS CDPP measurements, and the gold curve is a moving median of the 1-hr uncertainties.

Table 3: Sector Fireflies and Fireworks

FFI Start	FFI End	Cameras	Description
2019120172932	2019120175932	2,3	Fireflies
2019125175932	2019125182932	4	Firefly
2019125192932	2019125195932	2,3,4	Fireflies
2019135162932	2019135165932	2,3,4	Fireflies
2019136155932	2019136162932	1,2,3,4	Fireworks
2019137122931	2019137125931	1	Fireflies

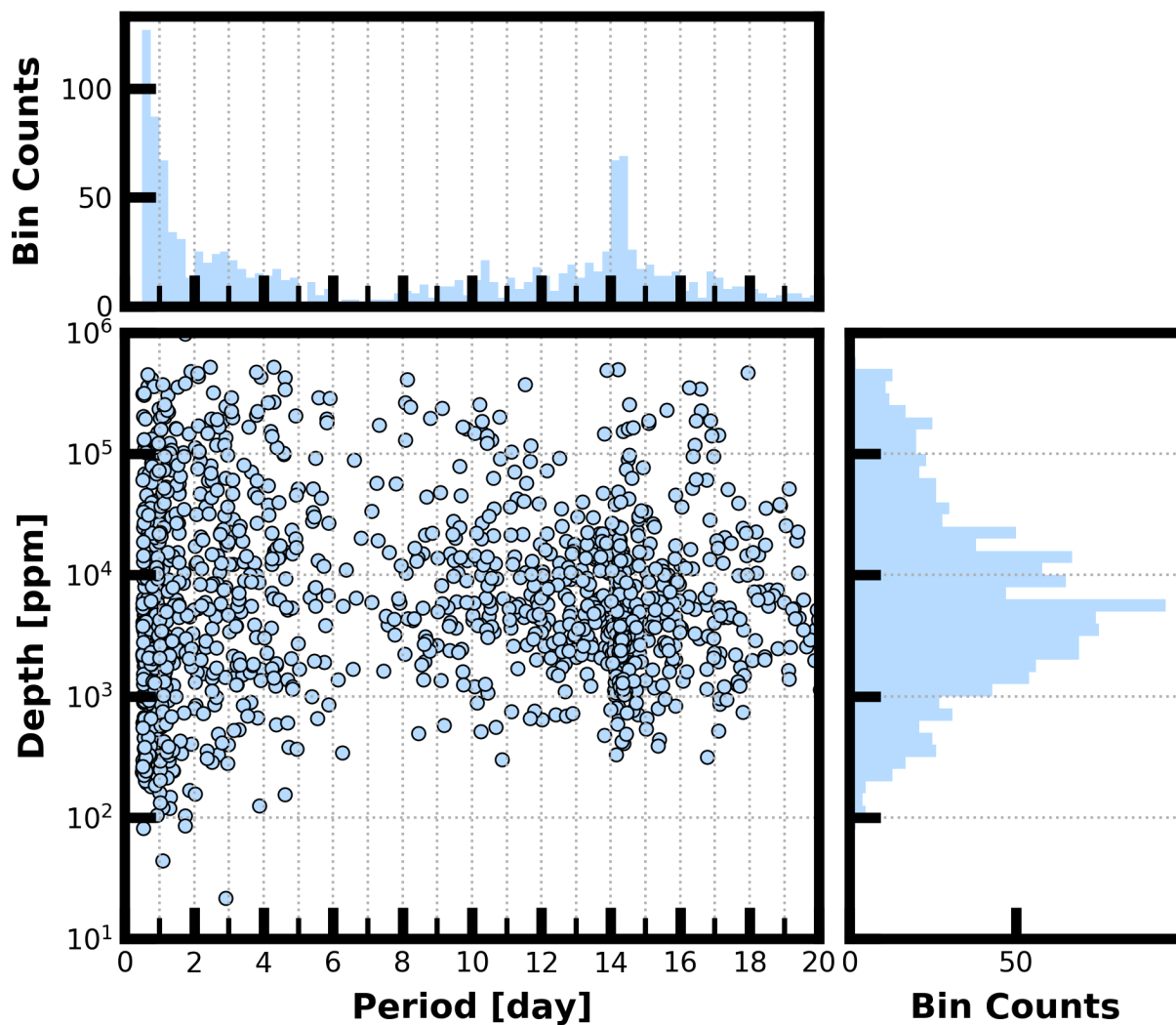


Figure 7: Lower Left Panel: Transit depth as a function of orbital period for the 1648 TCEs identified for the Sector 11 search. For enhanced visibility of long period detections, TCEs with orbital period < 0.5 days are not shown. Reported depth comes from the DV limb darkened transit fit depth when available, and the DV trapezoid model fit depth when not available. Top Panel: Orbital period distribution of the TCEs shown in the lower left panel. Right Panel: Transit depth distribution for the TCEs shown in the lower left panel.

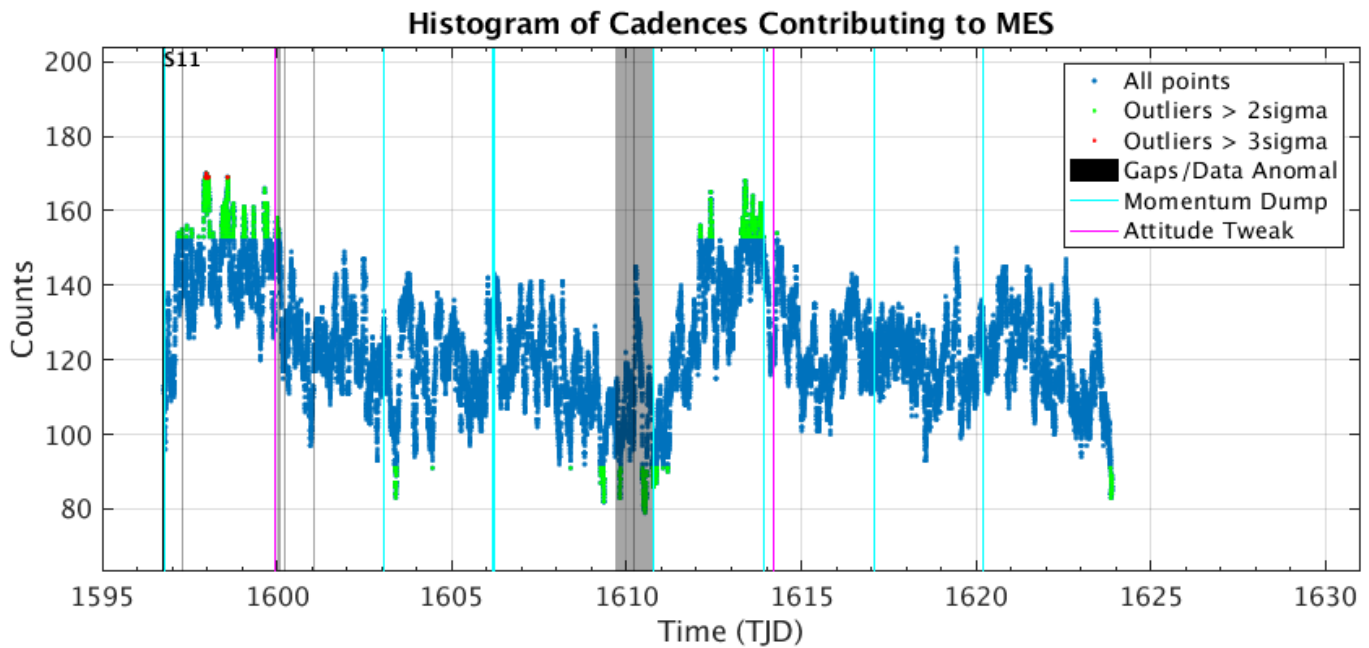


Figure 8: Number of TCEs at a given cadence exhibiting a transit signal. Isolated peaks are caused by a single event and result in spurious TCEs. The peaks typically align with pointing instabilities and strong background variations.

Table 4: Sector 11 TCE Numbers

Number of TCEs	Number of Targets	Total TCEs
1	839	839
2	289	578
3	54	162
4	12	48
5	3	15
6	1	6
–	1198	1648

References

- Jenkins, J. M. 2017, Kepler Data Processing Handbook: Overview of the Science Operations Center, Tech. rep., NASA Ames Research Center
- Jenkins, J. M., Twicken, J. D., McCauliff, S., et al. 2016, in Proc. SPIE, Vol. 9913, Software and Cyberinfrastructure for Astronomy IV, 99133E
- Li, J., Tenenbaum, P., Twicken, J. D., et al. 2019, *PASP*, 131, 024506
- Twicken, J. D., Catanzarite, J. H., Clarke, B. D., et al. 2018, *PASP*, 130, 064502
- Vanderspek, R., Doty, J., Fausnaugh, M., et al. 2018, TESS Instrument Handbook, Tech. rep., Kavli Institute for Astrophysics and Space Science, Massachusetts Institute of Technology

Acronyms and Abbreviation List

BTJD	Barycentric-corrected TESS Julian Date
CAL	Calibration Pipeline Module
CBV	Cotrending Basis Vector
CCD	Charge Coupled Device
CDPP	Combined Differential Photometric Precision
COA	Compute Optimal Aperture Pipeline Module
CSCI	Computer Software Configuration Item
CTE	Charge Transfer Efficiency
Dec	Declination
DR	Data Release
DV	Data Validation Pipeline Module
DVA	Differential Velocity Aberration
FFI	Full Frame Image
FIN	FFI Index Number
FITS	Flexible Image Transport System
FOV	Field of View
FPG	Focal Plane Geometry model
KDPH	Kepler Data Processing Handbook
KIH	Kepler Instrument Handbook
KOI	Kepler Object of Interest
MAD	Median Absolute Deviation
MAP	Maximum A Posteriori
MAST	Mikulski Archive for Space Telescopes
MES	Multiple Event Statistic
NAS	NASA Advanced Supercomputing Division
PA	Photometric Analysis Pipeline Module

PDC Pre-Search Data Conditioning Pipeline Module

PDC-MAP Pre-Search Data Conditioning Maximum A Posteriori algorithm

PDC-msMAP Pre-Search Data Conditioning Multiscale Maximum A Posteriori algorithm

PDF Portable Document Format

POC Payload Operations Center

POU Propagation of Uncertainties

ppm Parts-per-million

PRF Pixel Response Function

RA Right Ascension

RMS Root Mean Square

SAP Simple Aperture Photometry

SDPDD Science Data Product Description Document

SNR Signal-to-Noise Ratio

SPOC Science Processing Operations Center

SVD Singular Value Decomposition

TCE Threshold Crossing Event

TESS Transiting Exoplanet Survey Satellite

TIC TESS Input Catalog

TIH TESS Instrument Handbook

TJD TESS Julian Date

TOI TESS Object of Interest

TPS Transiting Planet Search Pipeline Module

UTC Coordinated Universal Time

XML Extensible Markup Language